Viscoelastic damping design – A novel approach for shape optimization of Constrained Layer Damping treatments at different ambient temperatures

Martin Gröhlich [a,b] *, **Marc Böswald** [a,b], **Jörg Wallaschek** [c]

[a] German Aerospace Center (DLR), Institute of Aeroelasticity
Bunsenstraße 10, 37073 Göttingen, Germany

[b] Cluster of Excellence SE²A – Sustainable and Energy-Efficient Aviation, Technical University Braunschweig, Germany

[c] Leibniz University Hannover, Institute of Dynamics and Vibration Research (IDS)
An der Universität 1, 30823 Garbsen, Germany

Keywords:
constrained layer damping; viscoelastic damping design; geometric shape optimization

Abstract

Constrained Layer Damping (CLD) is an effective technique for passive damping of bending vibrations. By placing viscoelastic material in between a base and face layer, the resulting shear strain dissipates the vibrational energy due to the properties of the material. However, the damping performance of such treatments depends highly on the location and shape of the added layers as well as on the mechanical properties of the viscoelastic material. This paper addresses the shape optimization of CLD in beams. The objective of the optimization is to achieve maximum damping for a set of a-priori selected modes at different ambient temperatures. A gradient-free optimization approach is used, which allows to determine the optimal width of core and face layer on an unchanging finite element mesh under mass constraints. As a test case for the algorithm, a CLD beam made of aluminum and an elastomeric bromobutyl-rubber mixture is studied. In order to validate model and algorithm, the simulation results are compared to experimental results, which were obtained by impact testing. The results demonstrate that the proposed method is a powerful tool for shape optimization of CLD. Furthermore, the temperature has a considerable influence on the optimal design. As a consequence, proper attention should be paid to the specification of operating conditions, in particular with respect to the expected temperature.

1 Introduction

Passive vibration damping plays a key role in the design of lightweight structures, in particular in aeronautics and in the design of aircraft components. Since lightweight structures are prone to vibration, the design process is dominated by strict aeroelastic and fatigue requirements. With regard to vibration, a distinction can be made between safety-relevant and comfort-relevant vibrations. For instance, wing vibrations as a result of gust encounter can impair the controllability of an aircraft. Furthermore, fuselage vibrations are caused e.g. by the turbulent boundary layer, by vortex shedding in the wake of antennas or by the transmission of structure borne sound from operating systems such as engines, hydraulic pumps, electric power generator or air condition systems. All these examples have in common that the associated vibrations

* Corresponding author. Tel.: +49 551 709 2366.
E-mail address: Martin.Groehlich@dlr.de

have an adverse effect on the acoustic comfort of the passengers. Airframes are mainly composed of shell structures with thin plates, stiffened by beam-like components, such as stringers, spars and frames. In most cases, damping is not considered in the initial design phase of such structures. Since a fair amount of damping is beneficial to the dynamic behavior of the airframe, a general interest exists in the damping of bending vibrations.

In this context, viscoelastic materials have been studied for decades [1]. Constrained Layer Damping (CLD) treatments have been identified as an effective means for vibration damping. A CLD treatment, regardless if applied to beam- or plate-type systems, consists of a soft viscoelastic layer that is constrained between the host structure and a stiff face layer. If the sandwich structure experiences bending deformation, the viscoelastic material is forced into shear strain. Due to its dissipative properties, the viscoelastic material transforms vibration energy into thermal energy, thus contributing to an increase of damping and consequently to a faster decay of the vibration. Additionally, higher damping also leads to a reduction of the steady-state amplitude of harmonically excited systems. In general, the damping performance is linked to the material properties and geometric shape of the treatment. In many engineering cases, mass limits truncate the design space, forcing the engineer to find the most efficient design for maximum damping of a particular mode or temperature. This paper is dedicated to the shape optimization of CLD treatments in order to get the best damping performance from the added damping treatment. Variation of thermal conditions plays an important role in the design of viscoelastic damping and will be taken into account in the shape optimization.

1.1 Literature review

The origin of the technology of CLD treatments can be traced back to the work of Oberst and Frankenfeld [2]. The authors analyzed metallic sheets with an attached viscoelastic layer. In this composition, which is known as Free Layer Damping (FLD), the viscoelastic layer experiences extensional strain and dissipates energy in this way. Based on their approach, Kerwin realized the potential of forced shear strain in the viscoelastic layer and developed a three-layer sandwich construction [3]. This setup, known as CLD, enables higher damping capability compared to FLD. In this regard, Ross et al. proposed the Ross-Kerwin-Unger method for analyzing the dynamic performance of CLD beams [4]. Kerwin's approach was taken up by Di Taranto who developed an analytical sixth-order differential equation for freely vibrating CLD beams accounting for any boundary condition [5]. Mead and Markus extended Di Taranto's work by including a formulation of the transverse displacement into the analytical model [6]. Applying an energy-based approach, Rao provided analytical models for CLD beams under various boundary conditions [7]. All these analytical models assumed a uniform width of the layer of the CLD components and served as a basis for damping optimization. For instance, Lifshitz and Leibowitz presented an optimization algorithm for the determination of the optimal layer thicknesses with additional design constraints [8].

However, advances in this area were strongly linked to the availability of analytical models and the application of such analytical formulations to complex and assembled structures was difficult. Only the increasing application of the finite element method (FEM) led to more efficient damping analysis methods and improved design opportunities. While the geometric dimensions such as length and thicknesses of the layer or material properties were mostly considered as design parameters in the past, alternative parameters such as location of single CLD patches became available. Amongst others, Marcelin et al. optimized the dimensions and locations of CLD patches on FE-beam structures for maximizing the modal loss factor by means of the Method of Moving Asymptotes (MMA) and a genetic algorithm, respectively [9, 10]. The MMA is a popular structural optimization method that substitutes a constrained optimization problem by a strictly convex and approximated subproblem [11]. In contrast to it, Alvelid used the gradient of the objective function to identify appropriate elemental locations for adding constrained damping material to a vibrating structure [12]. The result was a shape optimization process, where the final design evolved step by step. As an alternative approach, Lepoittevin and Kress optimized cut positions for segmenting full coverage CLD treatments [13]. In this way a higher shear deformation in the viscoelastic core layer and thus an increased modal loss factor of the structural vibration could be achieved. Considering viscoelastic laminated composite sandwiches, Araújo et al. optimized the elastic ply orientation angles and thicknesses of different layers by a gradient based optimization [14]. Based on this work, Madeira et al. included

additional design variables such as the amount and the type of material of the layers [15]. They performed a multiobjective optimization, maximizing modal damping factor and minimizing material costs and weight simultaneously.

In the recent years, the application of structural topology optimization became increasingly popular. Using MMA, Ling et al. determined the optimal viscoelastic material topology of a plate to be covered afterwards by CLD [16]. The authors considered different boundary conditions and showed that an appropriate material distribution leads to a significant reduction of the structural response. Kim et al. carried out a topology optimization of a viscoelastic layer attached to a curved shell structure with regard to maximum damping [17]. The results were compared to the damping values resulting from energy- and mode shape-based approaches for optimal damping material placement. Also applying the MMA, Zheng et al. were the first to perform a topology optimization based on CLD elements for different plate structures [18]. For this purpose, the authors established an interface finite element and, in this way, reduced the numerical effort. Furthermore, Fang and Zheng applied topology optimization to plates with CLD treatment and used a modified sensitivity analysis [19]. They validated their numerical results by an experiment, demonstrating a decrease of the resonant response of a targeted mode. The latest advances encompass the work of Zhang et al. who introduced a hierarchical optimization algorithm for minimizing the sound radiation power of plates with CLD material [20]. The algorithm consists of an evolutionary structural optimization method, for determining the position of the material and of a genetic algorithm, for calculating the material thicknesses.

1.2 Objective and content of the paper

As presented in the literature review, many researchers have contributed to the problem of viscoelastic damping optimization. The usual design parameters have been the thicknesses and placements of core and face layer, but also cut positions and ply angles. Furthermore, sensitivity-based topology optimization became popular in recent years. Nevertheless, the state-of-the-art still reveals some knowledge gaps which are addressed in this paper:

- The width of the core and face layer of CLD beams have been rarely considered as design parameters for shape optimization. The idea behind the following approach is motivated by a previous work of Gröhlich et al. [21]. Using a parameter study, the authors have demonstrated that the damping performance of a CLD beam can be significantly influenced by adjusting the width of the core and face layer.

- For optimization, gradient-based or gradient-free methods can be applied. Depending on the respective application and on the analysis time which is required for the considered model, one method can be more advantageous than the other. A particular difficulty for frequency dependent viscoelastic materials is that the calculation of the sensitivities can be cumbersome. A gradient-free shape optimization method, accounting for an additional mass constraint, circumvents this problem.

- In most optimization problems, constant viscoelastic material properties are applied. However, real viscoelastic materials such as elastomers exhibit a strong dependence on frequency and temperature. Until now it has not been analyzed, if and how the optimal design of a CLD beam depends on temperature. And it has also not yet been analyzed, if an optimal design, which is calculated for a particular temperature, also delivers decent damping if temperature changes over a wide range.

The content of the paper is structured as follows: In Chapter 1, an introduction was given and important contributions to the field of CLD treatments were reviewed. The fundamentals of frequency and temperature dependent viscoelastic material modeling and corresponding analysis methods will be exemplified in Chapter 2. Chapter 3 presents a new approach of a gradient-free algorithm for shape optimization of CLD beams regarding maximum damping. The structure of the algorithm is explained and demonstrated by means of an example with two design variables. In Chapter 4, the algorithm is analyzed with respect to the trade-

off between numerical cost and precision of results. Chapter 5 is about the application of the algorithm to a CLD beam with a fully characterized bromobutyl-rubber mixture. The influence of different temperatures on the optimal design is analyzed and the result is experimentally validated. In Chapter 6, the central points of this paper are summarized and the main conclusions are drawn.

2 Theoretical background of viscoelastic damping

In this section, the fundamentals of viscoelastic damping are briefly discussed. A comprehensive overview of the basic theory can be found in [22, 23, 24, 25]. More detailed information and important advances are reviewed and reported in the work of Vasques et al. [26] and Zhou et al. [27].

2.1 Viscoelastic material modeling

Viscoelastic materials are known to exhibit frequency and temperature dependent behavior. Under the assumption of harmonic steady-state excitation, the linear viscoelastic properties can be expressed in terms of a complex modulus E^*

$$E^*(\omega, T) = E'(\omega, T) + iE''(\omega, T). \tag{1}$$

The elastic part is indicated by the storage modulus E', while the loss modulus E'' describes the dissipative part. Furthermore, ω is the angular frequency, T the Temperature and i the imaginary unit. The key parameter for assessing the damping capability of a linear viscoelastic material is the ratio of loss and storage modulus, denoted as material loss factor $\tan(\delta)$

$$\tan(\delta(\omega, T)) = \frac{E''(\omega, T)}{E'(\omega, T)}. \tag{2}$$

Different approaches are reported in the literature for modelling the frequency dependence of viscoelastic materials. In addition to the model of fractional derivatives [28] and the GHM-model [29], the modeling is often performed by means of a generalized Maxwell-model [23]. In the latter case, the storage and loss moduli are defined as a Prony-series consisting of several relaxation times τ_i and elastic moduli E_i resulting from curve fitting of measurement data

$$E'(\omega) = E_\infty + \sum_{i=1}^{n} E_i \frac{\omega^2 \tau_i^2}{1 + \omega^2 \tau_i^2}, \tag{3}$$

$$E''(\omega) = \sum_{i=1}^{n} E_i \frac{\omega \tau_i}{1 + \omega^2 \tau_i^2}. \tag{4}$$

In eq. (3) the parameter E_∞ is called the long-term modulus and corresponds to the elastic behavior at quasi-static deformation ($\omega \to 0$). It should be emphasized that a complex shear modulus G^* is often used for the representation of the material properties in literature. Under the assumption of isotropy and by applying Poisson's ratio ν, the following relation is prevalent

$$E^* = 2G^*(1 + \nu). \tag{5}$$

Due to the chemical composition of viscoelastic materials such as elastomers, an analogy exists between the frequency and temperature dependence. The mechanical behavior at small frequencies is similar to that at high temperatures and vice versa. This phenomenon known as time-temperature superposition allows for shifting the frequency dependent material curves, thus determining the material properties at arbitrary temperatures. For rheological simple materials, the shifting along the frequency axis can be performed by a horizontal shift factor a_T, resulting from the Williams-Landel-Ferry (WLF) equation [30]

$$\log_{10}(a_T) = \frac{-C_1 \cdot \Delta T}{C_2 + \Delta T} \tag{6}$$

The parameters C_1 and C_2 are fitting parameters and ΔT is the difference between the actual and the reference temperature ($\Delta T = T - T_{ref}$). For instance, the loss modulus at a reference temperature T_{ref} and at a reference frequency f_{ref} is the same as at an arbitrary temperature T and a frequency $f = a_T \cdot f_{ref}$. If the elastomer is filled with carbon black, the Payne effect [31, 32] occurs which is incorporated in the time-

temperature analogy by an additional vertical shift. The vertical shift is considered as an Arrhenius-like activation process and the corresponding shift factor b_T can be calculated by the apparent activation energy E_A and the universal gas constant R, with e as Euler's number [33]

$$b_T \approx e^{-\frac{E_A}{R \cdot \Delta T}}. \tag{7}$$

Finally, the material properties at arbitrary temperature and frequency can be determined by incorporating both shift factors

$$\begin{aligned} E'(f,T) &\rightarrow b_{T,E'} \cdot E'(a_T \cdot f_{ref}, T_{ref}) \\ E''(f,T) &\rightarrow b_{T,E''} \cdot E''(a_T \cdot f_{ref}, T_{ref}). \end{aligned} \tag{8}$$

It should be noted that the activation energies for storage and loss modulus might be different. For more detailed information about the chemical background and the application of the shift process, the interested reader is referred to [34].

2.2 Analysis method

The forced structural vibration of a system which is composed of elements with viscoelastic properties is usually described by the equation of motion in the frequency domain [24]

$$[-\omega^2 \boldsymbol{M} + \boldsymbol{K}^*(\omega)]\boldsymbol{u}^* = \boldsymbol{F} \tag{9}$$

Here, $\boldsymbol{M}$ denotes the mass matrix, $\boldsymbol{u}^*$ the vector of the complex amplitudes of generalized coordinates and $\boldsymbol{F}$ the complex force amplitudes of the harmonic load, acting on the structure. The frequency dependent viscoelastic material properties are propagated through the FE formulation, resulting in a complex and frequency dependent stiffness matrix $\boldsymbol{K}^*$. More information regarding the basic FE theory can be found in [35] and details, in particular about the composition of the complex stiffness matrix, are addressed in [34]. From eq. (9) it gets clear that, due to the frequency dependent stiffness matrix, the eigenvalue problem for the free vibration ($\boldsymbol{F} = \boldsymbol{0}$) is not directly solvable. However, this difficulty can be circumvented by the use of appropriate analysis methods. Some of these methods are reported and reviewed by Vasques et al. [26] and compared by Rouleau et al. [36]. In the following, we will apply an iterative eigenvalue solver (IES) whose constitutive algorithm is based on the secant method as described in [34, 37]. At this point it should be noted that the eigenvalue λ_r of the rth mode resulting from a viscoelastically damped system has to be interpreted differently than the eigenvalue of a viscously damped vibration [38]

$$\lambda_r^2 = \omega_r^2(1 + i\eta_r). \tag{10}$$

Basically, the real part contains the information about the eigenfrequency ω_r, while the damping in terms of the modal loss factor η_r is obtained by the ratio of imaginary and real part

$$\eta_r = \frac{\lambda_{r,imag}^2}{\lambda_{r,real}^2} \tag{11}$$

It is worth to emphasize the difference between the modal loss factor and the material loss factor. While the modal loss factor denotes the damping of the mode of a system and is thus a system property, the material loss factor indicates the material damping capacity which is independent of the properties of the system where this material is applied. Furthermore, for weakly damped systems, an analogy exists to the viscous damping ratio D_r by $2D_r \approx \eta_r$, making the evaluation of the modal loss factor more comprehensible and practical.

3 A gradient-free algorithm for shape optimization

This section addresses the theory of the chosen optimization technique and introduces the corresponding algorithm. For a better overview, the algorithm is subdivided into one main part and two secondary parts, the design loop and the mass constraint handling, respectively. In the end, an illustrative example is given.

3.1 Formulation of the structural optimization problem

The objective of the optimization algorithm is to maximize the damping of a vibrating CLD-beam under predefined mass and geometrical constraints. The FE grid of the host structure remains unchanged during the optimization with a fixed number of elements in longitudinal and transverse direction. Additionally, a symmetry axis is drawn along the longitudinal axis. Starting from the symmetry axis, finite elements of the viscoelastic core and the metallic face layer are simultaneously added to the left and to the right of the symmetry axis, while each element group in longitudinal direction defines a potential design variable x_j. A value of $x_j = 0$ means that no CLD material is added and a value of $x_j = 2$ adds two CLD elements left and right of the symmetry axis. An advantage of this approach is that several elements can be merged as one design variable, thus reducing the computational effort. Moreover, symmetry effects of the vibration modes can be used to further simplify the problem. An example of this procedure will be shown later in Section 3.5. In the end, the general optimization problem can be expressed as a minimalization task

$$\begin{aligned} &\text{Minimize:} && -\eta_r(\boldsymbol{x}) \\ &\text{Subject to:} && m_{CLD}(\boldsymbol{x}) - m_{bound} \leq 0 \\ & && x_{min} \leq x_j \leq x_{max} && \text{for } j = 1,\dots,n \\ & && && x_j \in \mathbb{N} \end{aligned} \tag{12}$$

where m_{CLD} is the actual mass of the system, m_{bound} is the permitted mass, $\boldsymbol{x}$ is the vector of n design variables x_j and x_{min} and x_{max} are geometrical limits. Due to the discrete FE grid, the design variables can be only positive integer numbers.

3.2 Basic structure of the optimization algorithm

The above-mentioned objective is achieved by finding the optimal distribution of the width of the core and face layer on a constant FE grid. For this purpose, an optimization technique has been developed which is similar to the Gauss-Seidel method and is thus denoted as modified Gauss-Seidel (MGS) method in the following. Figure 1 shows the basic structure of the algorithm. In general, the presented method can be subdivided into two parts: The constitutive algorithm with a design loop and the mass constraint handling. It should be noted that in case of a structural optimization, the objective function is a complex composition of many subprocess. Such processes encompass e.g. the regeneration of the FE mesh, an eigenvalue analysis as well as a mode-tracking algorithm.
The algorithm starts with initial design variables $\boldsymbol{x}_s$ and the corresponding objective function value η_s. As a first step, this data set is utilized in the design loop to find improved design variables $\boldsymbol{x}_{imp}$. The improved data set is forwarded to the mass constraint handling afterwards, checking the violation of present mass constraints. Finally, the optimal design variables $\boldsymbol{x}_{opt}$ are available and are proven regarding convergence.

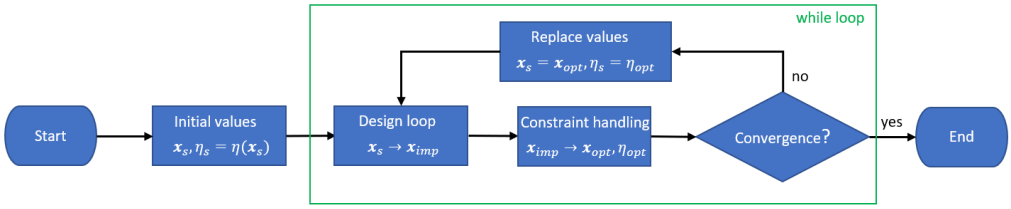

Figure 1: Basic structure of the optimization

3.3 Design Loop

The key part of the algorithm is the design loop which is therefore separately presented in Figure 2. For every step in the For-loop, a copy $\tilde{\boldsymbol{x}}$ of the current design variable vector is built. It is checked afterwards, if an increase of the j[th] design variable would violate the corresponding maximum geometric limit. If not, the change is adopted and the modified design variables are evaluated in the objective function, leading to a temporary value of the modal loss factor $\tilde{\eta}$. In case the change causes an improvement of the objective function value, both values are saved for later use in the corresponding vectors $\boldsymbol{x}_{imp}$ and $\boldsymbol{\eta}_{imp}$. If no improvement is achieved or if an increase of a design variable violates the upper geometric limit, it is proven, whether a reduction of the design variable value is feasible. If this is true and if the modified design represents an improvement, the changes are adopted and saved. If any of these conditions is false, the changes are rejected and the initial values are adopted. After finishing the loop, the vector $\boldsymbol{x}_{imp}$ contains all single geometric modifications while the vector $\boldsymbol{\eta}_{imp}$ contains the corresponding modal loss factors.

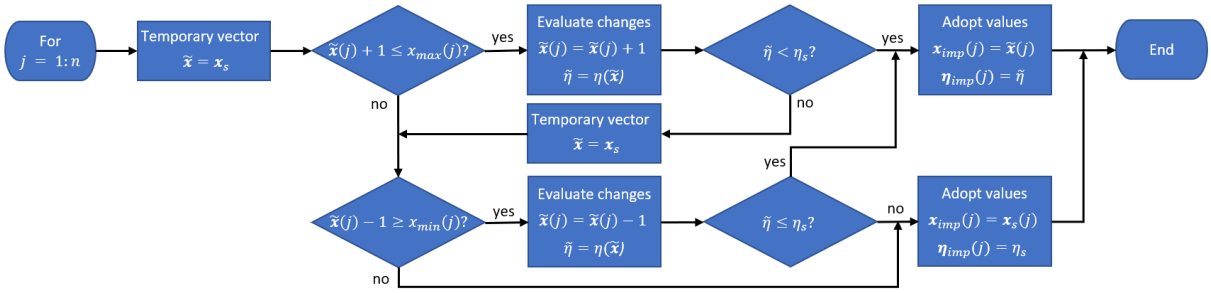

Figure 2: Flowchart of the design loop algorithm

It should be mentioned that the part denoted “evaluate changes” in Figure 2 actually means the analysis of the FE-Model with the current setting of the design variables. This is the costly part of the optimization.

3.4 Mass constraint handling

Five different scenarios can occur during the mass constraint handling. The corresponding flowchart is plotted in Figure 3 and the scenarios are described below. The mass constraint function is denoted as $c(\boldsymbol{x})$.

1. **Constraint is not violated**
   When the mass constraint is not violated, it still needs to be proven, whether applying all single improvements together leads to an overall improvement of the modal loss factor. If this is true, the geometric changes are adopted. If not, the improvements of the single modifications are ranked regarding their impact on the modal loss factor and the changes are sequentially reset, starting from the worst improvement. This loop is stopped when an improvement of the objective function value is achieved.

2. **Constraint is violated and at least one design variable is lower compared to the previous state**
   If the mass constraint is violated, it is checked, if any of the improved design variables are lower compared to the previous step. This would mean that elements are removed and the mass condition is inevitably met. In this case, the corresponding improved “removing” design variable is adopted and all other improvements are rejected ($\boldsymbol{x}_{imp} \rightarrow \boldsymbol{x}_{remove}$). If the above-mentioned condition applies to more than one design variable, all improved “removing” design variables are temporary adopted. However, the adoption of multiple design variables might cause the modal loss factor to decrease and needs to be checked. If an improvement is confirmed, the adoption is valid. Otherwise, only the “removing” modification, causing the best improvement of the modal loss factor is adopted.

3. **Constraint is violated and no design variable is lower compared to the previous state**

If the improved design variable vector does not contain "removing" design variables, the design changes are ranked regarding their improvement of the modal loss factor ($\boldsymbol{x}_{imp} \rightarrow \boldsymbol{x}_{rank}$). Afterwards, the increase of each design variable is subsequently reset, starting with the worst. This procedure is repeated until the mass condition is met ($\boldsymbol{x}_{rank} \rightarrow \boldsymbol{x}_{reset}$). If the resulting configuration is an improvement compared to the one of the previous loop, the design variables are adopted.

4. **Constraint is violated, removal of single design variables did not yield an improvement**
   Scenario 4 works as follows: A reduction technique is applied based on the ranked design variable vector $\boldsymbol{x}_{rank}$. For this purpose, only the design variable leading to the best improvement is kept and the others are rejected and set back to the state of the previous loop. Then, the "worst" design variable x_w is handled as a free parameter, while the other design variables are fixed. As a consequence, the mass constraint condition is transformed into a single variable function ($c(\boldsymbol{x}) \rightarrow c(x_w)$) and the worst design variable is systematically reduced by

$$x_{w,k+1} = x_{w,k} - 1 \tag{13}$$

   until the mass condition is met. In eq. (13), k indicates the k[th] step within the reduction method. By this procedure it is guaranteed that the mass condition is met. Afterwards, the new design vector is evaluated and it is verified, if an improvement is achieved. If not, the second worst design variable is chosen as the free parameter and the reduction method is applied again. The same applies, if a design variable crosses the lower boundary in the process of the reduction method. This procedure is repeated until the (n-1)[th] worst design variable or until an improved modal loss factor is achieved. In the end, the improved values are adopted as optimal parameters.

5. **Constraint is violated and reduction method does not yield a feasible improvement**
   If the constraint is violated and the reduction method does not lead to a feasible improvement, the initial values are adopted as optimal values, leading to termination of the MGS algorithm.

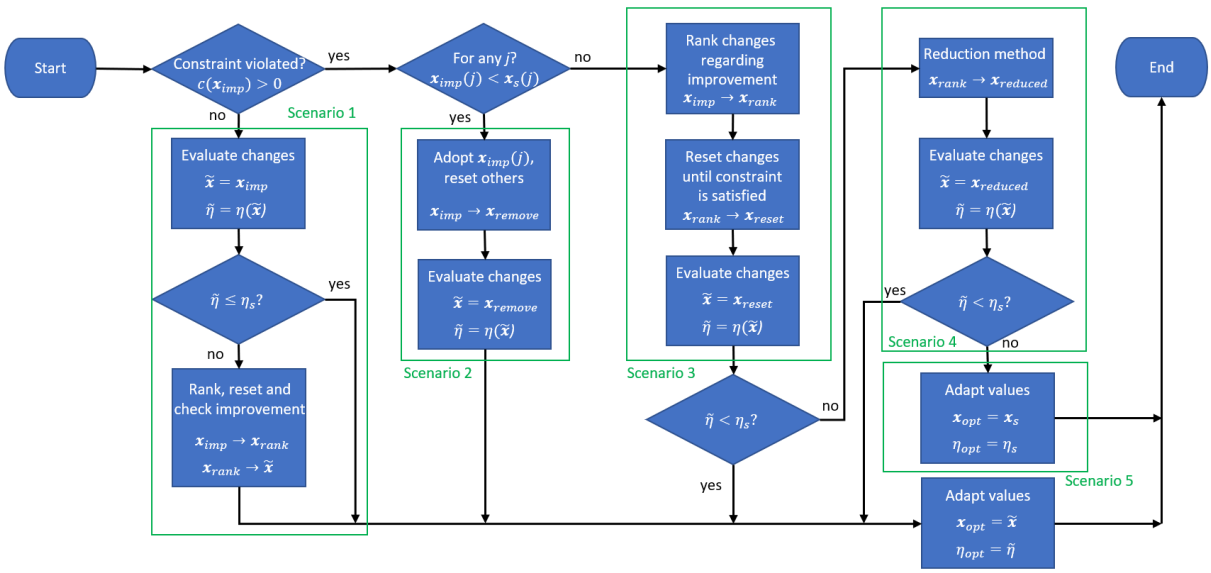

Figure 3: Flowchart of the mass constraint handling

3.5 Illustrative example

An example with two design variables is presented in the following, demonstrating the application of the modified MGS algorithm on a free-free vibrating CLD beam structure. MSC Nastran is used as a FE solver

and the algorithm is programmed in MATLAB. As an objective, the modal loss factor of the first bending mode is to be maximized. Additionally, a constraint is defined, limiting the coverage with CLD material to 50% of the upper surface of the beam. Since the first bending mode is symmetric to the bending axis, the symmetry is used for reducing the number of design variables and thus reducing the numerical effort. As a consequence, the two design variables x_1 and x_2 represent the width of the inner and outer layers, respectively. Both segments are of the same size, as illustrated in Figure 4. The structure is regularly modeled by 80 CHEXA solid elements in longitudinal (400 mm) and 40 elements in transverse (40 mm) direction with one element per layer in thickness direction. From that it follows that x_1 includes element sections 1-20 and 61-80 and x_2 includes element sections 21-60. The corresponding properties of the sandwich structure are listed in Table 1. In the first instance, the properties of the viscoelastic layer remain constant. This assumption differs from real material behavior but is considered acceptable for the demonstration of the algorithm. It should also be noted that core and face layer elements at the same position are always added or removed at the same time and do not overlap the base layer.

As an initial design vector, $\boldsymbol{x}_s = [8 \quad 0]^{\mathrm{T}}$ is chosen. Due to the symmetry line in length direction, the design variables correspond to a width of 16 mm for the outer and 0 mm for the inner layer. Figure 5(a) displays the iteration path with the corresponding convergence diagram (b). The optimization ends after 17 iterations with an optimal design vector of $\boldsymbol{x}_{opt} = [4 \quad 16]^{\mathrm{T}}$ and a modal loss factor of $\eta_{opt} = 0.1336$. The optimal widths are 8 mm for the outer and 32 mm for the inner layer as illustrated in Figure 6.

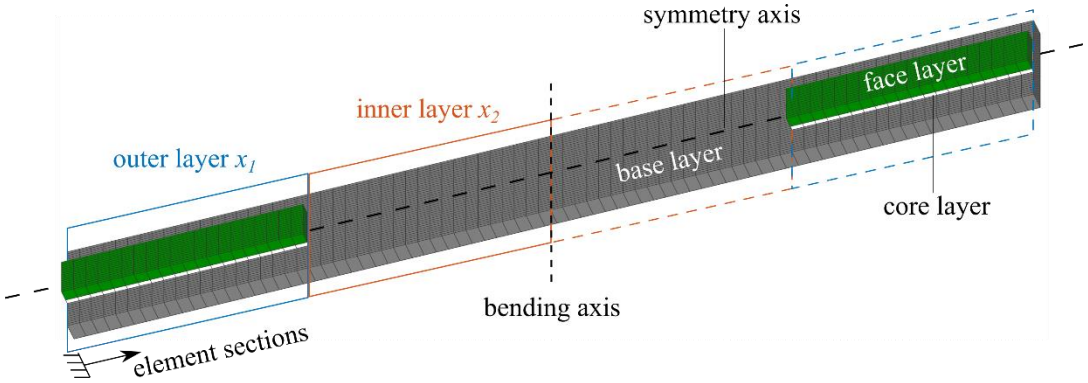

Figure 4: Initial design of the CLD beam and definition of inner and outer layer. The white layer corresponds to the viscoelastic core layer, while the face layer is colored in green.

Table 1: Properties of the CLD layers

	Density $\left[\frac{\mathrm{kg}}{\mathrm{m}^3}\right]$	Storage modulus [GPa]	Poisson's ratio [-]	Material loss factor [-]	Thickness [mm]
Base layer	2660	70	0.33	0.005	8
Core layer	1114	0.1	0.499	0.4	2
Face layer	2660	70	0.33	0.005	5

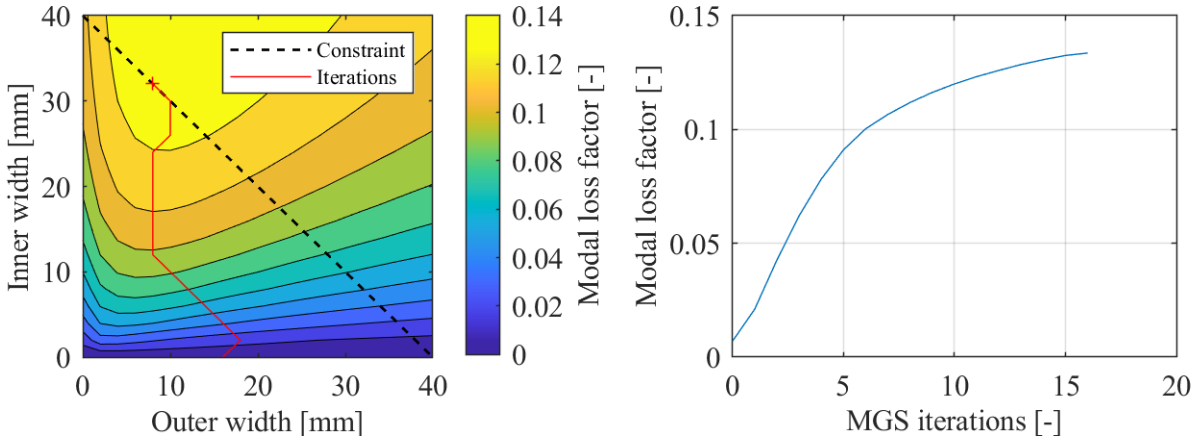

(a) (b)

Figure 5: (a) Iteration path from start point to maximum and (b) corresponding convergence diagram

Figure 6: Top: Optimal design of the first bending mode from top view. Black color indicates added core and face layers. Bottom: Mode shape of first bending mode.

It can be seen that the optimal solution conforms with the solution of the contour plot. Moreover, the permitted mass increase is fully utilized. The reason for the resulting CLD shape can be explained as follows: Shear deformation is crucial to "activate" the damping properties of the viscoelastic material. In the case of the first bending mode, the highest shear strain occurs at the outer edges of the viscoelastic layer and is termed as the "edge effect" by Lepoittevin and Kress [13]. A high shear deformation is achieved by a flexible viscoelastic layer. However, if the shear stiffness of the viscoelastic layer is too flexible, the corresponding strain energy is far below the strain energy of the base and face layer. As a consequence, only a minor part of the strain energy can be dissipated via the viscoelastic material, resulting in poor damping. On the other hand, if the layer is too stiff, the reverse effect occurs. Since the shear stiffness is increased, the shear deformation decreases as a consequence and the strain energy of the viscoelastic layer is again below the level of the other layers. For achieving high damping performance, it is therefore necessary to find a compromise between these two extreme states. It must be considered that the shear stiffness of the viscoelastic layer depends on three parameters, as presented in terms of a simplified shear block in [34]. Accordingly, the shear stiffness can be increased by increasing the material stiffness (storage modulus) or the layer width and length, but also by reducing the layer thickness. In the present example, the viscoelastic material stiffness seems to be relatively high, so that the corresponding effect on the shear stiffness is compensated by slim core and face layers at the outer edges of the beam. Later, in Section 5.1, it is demonstrated that the optimal design changes with the viscoelastic material stiffness.

4 Properties of the MGS algorithm

This chapter addresses the properties of the MGS algorithm. The influence of the number and distribution of design variables on the optimized design and modal loss factor are analyzed. The meshed beam structure from Section 3.5 serves as the basis for the analyses. Unless otherwise specified, the material properties and geometric dimensions from Table 1 are applied.

4.1 Influence of the number of design variables on optimization results

In Section 3.5 the optimization was performed with two design variables to maximize the damping of the first bending mode. In the following it is analyzed, if an increased number of design variables improves the result of the optimization. Finally, it shall be determined if the increasing numerical effort is justified. For this purpose, the beam is split up into (a) four and (b) eight equally spaced sections symmetrically positioned around the axis of symmetry. This means that in the case of four design variables, each design variable includes 10 element sections. Since the path of the optimization depends strongly on the initial values, the start position is always the uncovered beam ($\boldsymbol{x}_s = \mathbf{0}$). The optimized design is presented in Figure 7 (a) and (b) and the corresponding modal loss factors as well as the number of objective function calls are listed in Table 2.

(a) (b)

Figure 7: Optimal Design of the (a) four and (b) eight variable optimization

Table 2: Optimization results for different numbers of design variables

Variables [-]	Modal loss factor [-]	Increase [%]	Obj. function calls [-]	Optimal design vector
2	0.1336	-	62	[4 16]
4	0.1394	4.34	121	[1 8 13 18]
8	0.1405	5.17	221	[0 3 6 9 12 15 17 18]

From Figure 7 it can be seen that in both cases an elliptical shape emerges for the optimal design, when the number of design variables is increased. The result can easily be compared to Figure 6 where the result with only two design variables is shown. The major part of the CLD material is added at locations of maximum bending moment (center of the beam), where also the modal strain energy of the host structure is maximum. This conforms to the approach of Kumar and Singh [39] who added single CLD patches at location with highest modal strain energy. However, the computational costs increase significantly. Doubling the number of design variables causes approximately a duplication of the objective function calls. On the other hand, the modal loss factor only increases slightly. In comparison to two design variables, eight variables cause a relative damping increase by 5.17%. A compromise might be to start with a low number of variables and continue the optimization with an increased number, whenever convergence is achieved. Alternatively, shape interpolation can be a useful tool for keeping the numerical effort low but approaching an optimal design.

4.2 Influence of the design variable distribution on optimization results

Another question arises about the transferability of the previous observations to higher modes. Basically, the first bending mode shape of the beam in free-free boundary conditions is similar to a half sine. However, the mode shapes of higher modes become more complex. In this case it seems necessary to also increase the number of design variables and to think about their distribution on the FE structure. This task is addressed in the following. Three different distribution approaches for the design variables are analyzed for the second and third bending mode:

(1) Separation at vibration nodes and anti-nodes
(2) Distribution on vibration nodes and anti-nodes
(3) Distribution according to equal element size (as shown in Section 3.5)

In this regard, Figure 8 shows the bending deflection of the uncovered beam for the second and third mode, depending on the grid points in longitudinal direction. It should be noted that the second bending mode is anti-symmetric regarding the center point, while the third mode is mirror-symmetric.

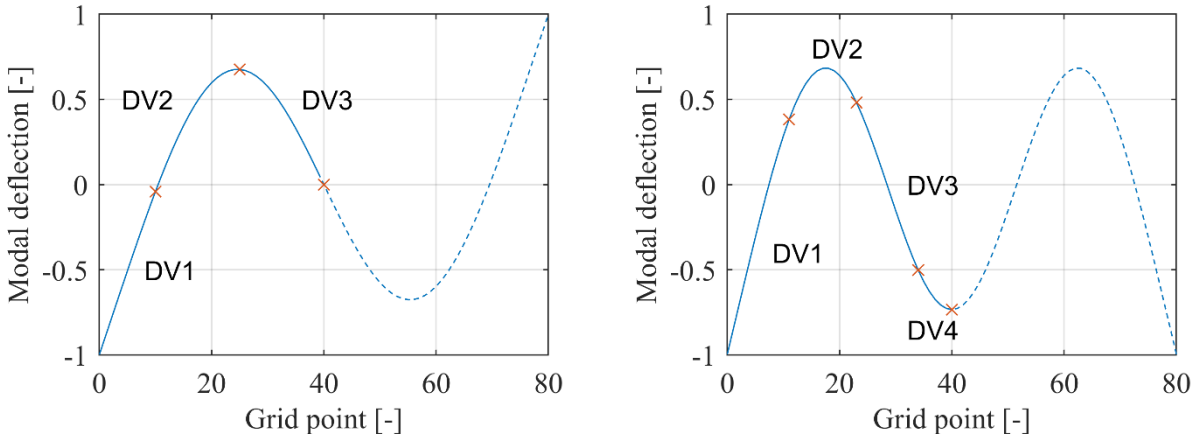

Figure 8: Modal bending deflection of (a) second and (b) third bending mode. Red markers indicate the position of design variable (DV) separation. In this context, (a) shows the DV separation of approach (1), while in (b) the DV separation of approach (2) is shown.

In this context, Table 3 and Table 4 list the element sections that belong to the corresponding design variables for the three different distribution approaches.

Table 3: Design variables and modal loss factor for the second bending mode

	Included element sections [-]				
Approach	DV 1	DV 2	DV3	DV4	Modal loss factor [-]
(1)	1-10 + 71-80	11-25 + 56-70	26-55	-	0.1144
(2)	1-5 + 76-80	6-16 + 65-75	17-34 + 47-64	35-46	0.1136
(3)	1-10 + 71-80	11-20 + 61-70	21-30 + 51-60	31-50	0.1150

Table 4: Design variables and modal loss factor for the third bending mode

	Included element sections [-]				
Approach	DV 1	DV 2	DV3	DV4	Modal loss factor [-]
(1)	1-7 + 74-80	8-18 + 63-73	19-28 + 53-62	29-52	0.0811
(2)	1-11 + 70-80	12-23 + 58-69	24-34 + 47-57	35-46	0.0862
(3)	1-10 + 71-80	11-20 + 61-70	21-30 + 51-60	31-50	0.0845

From Table 3 it gets clear that the highest modal loss factor for the second bending mode can be achieved, when distribution approach (3) with $\boldsymbol{x}_{opt} = [7\ 10\ 10\ 13]^T$ is applied. In contrast to it, distribution approach (2) with $\boldsymbol{x}_{opt} = [11\ 9\ 15\ 1]^T$ is the most promising for the third bending mode. The corresponding final designs are shown in Figure 9.

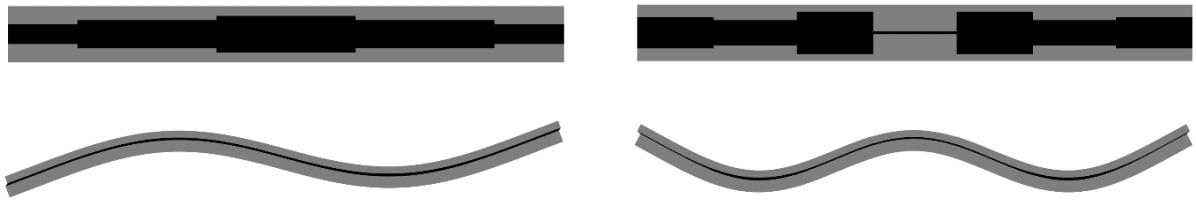

(a) (b)

Figure 9: Optimal design of the (a) second and (b) third bending mode from top view with the corresponding mode shapes

The optimal design for the second bending mode also insinuates an elliptical shape. The highest shear strain in the viscoelastic layer appears at the free ends and in the center. While the layer width is slim at the outer edges, it increases towards the center. In contrast to it, the optimal design for the third bending mode exhibits slimmest layers on the antinodes. In particular the design at the center anti-node is striking, since an extremely slim section appears. Nevertheless, this section is not superfluous - removing it reduces the modal loss factor relatively by 2.44%. Instead, the core and face layers are wider at the free ends and between the anti-nodes. It should be noted that the layer width at the outer edges increases for higher modes. This is due to the mode shape becoming more complicated, thus also increasing the strain energy in the elastic layers. The shear stiffness of the viscoelastic layer must be also increased in order to provide sufficient resistance to the deformation. This is achieved by adding CLD material to the location of maximum shear deformation. In this way, the strain energy in the viscoelastic layer is elevated closer to the level of the elastic layers, causing the modal loss factor to rise.

5 Application of the MGS algorithm

In this chapter, the application of the MGS on a CLD beam with a real viscoelastic material is demonstrated and experimentally validated. The damping material is a bromobutyl-rubber mixture (BIIR) that has already been applied successfully in previous studies [40, 41, 34]. The frequency and temperature dependent material behavior is fully characterized by Prony, WLF and Arrhenius parameters, as presented in Table A and Table B in the appendix. Two different temperatures ($T_1 = -20°C$ and $T_2 = 20°C$) are chosen for the design optimization. These temperatures are representative for the airframe temperature of a large transport aircraft during a flight. The upper thermal boundary represents the temperatures on ground. The lower thermal boundary considers the ambient temperature at flight altitude with some friction heating from the boundary layer around the airframe when flying at transonic speed. Figure 10 shows the storage modulus and the material loss factor as a function of frequency for both temperatures.

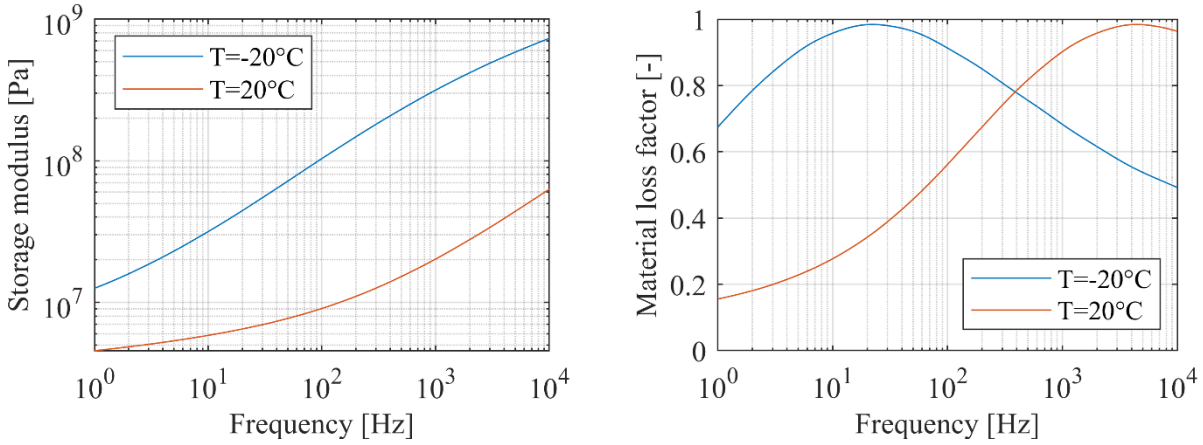

(a) (b)

Figure 10: (a) Shear storage modulus and (b) loss factor of BIIR for -20°C and 20°C

From Figure 10 it is evident that both, storage modulus and loss factor, vary considerably with frequency and temperature. The elastic material stiffness is low for low frequency and also for high temperatures. In contrast to it, the loss factor exhibits a maximum at low frequency for -20°C and at high frequency for 20°C. This region of significant change of elastic stiffness with temperature and maximum of loss factor is typically called the glass transition region of elastomeric material. In particular the storage modulus is a key parameter for achieving highest damping. However, a rule of thumb for a rough estimate of a suitable scale for the storage modulus does not exist, since it strongly depends on the dimension of the structure and its mode shapes. As it was shown by Gröhlich et al. [34], geometric adaption of the CLD layers can be used to compensate for an inappropriate viscoelastic storage modulus. In contrast, the material loss factor can be understood as a proportional factor for tuning the damping of a vibrating system – the higher it is, the higher the vibration damping.

5.1 Variation of storage modulus

Since material loss factor and storage modulus are coupled parameters in real elastomeric materials and change simultaneously with temperature and frequency, a clear distinction of the predominant parameter is hardly realizable. Therefore, in order to distinguish between the impacts of both material parameters, this section separately considers the influence of a storage modulus variation on the optimized design. For this purpose, the storage modulus of the viscoelastic material is changed to a constant value of $E' = 0.01$ GPa. As demonstrated in Figure 10, a modulus variation by a factor of 10 is possible in the considered temperature range. The other properties, in particular the material loss factor, remain as stated in Table 1. For the first and second bending mode, element distribution approach (3) of chapter 4.2 is applied and for the third mode

element distribution approach (2). The final designs (config. B) are illustrated and compared to the optimal designs based on a viscoelastic storage modulus of $E' = 0.1$ GPa (config. A) in Table 5.

Comparing the first modes, the design for the lower storage modulus (config. B) is inverted. The elliptical shape changed to an hourglass-like shape, where the major part of the CLD material is added at the free end of the beam and less material to the location of maximum bending moment and maximum modal strain energy, respectively. This observation complies with the explanation given in Section 3.5. Due to the lower viscoelastic material stiffness, the decrease in the shear stiffness of the layer is compensated by wider layer sections at the outer edges. The same applies to the second and third mode. Compared to config. A, the sections of maximum shear deflection are subsequently broadened, while the section belonging to the antinodes are thinned. Considering the third mode, the center "rod" completely disappeared. Instead, two thin rods emerge on top of the outer antinodes, forcing the adjacent wider damping patches into shear strain.

Table 5: Comparison of optimal designs for different storage moduli

Mode	Config.	Optimal design	Modal loss factor [-] $E' = 0.1$ GPa	Modal loss factor [-] $E' = 0.01$ GPa
1.	A		0.1394	0.0566
	B		0.0802	0.0816
2.	A		0.1150	0.0295
	B		0.0733	0.0371
3.	A		0.0868	0.0202
	B		0.0622	0.0205

By looking at the modal loss factor, an important observation can be made. CLD designs work less efficiently, if the viscoelastic storage modulus differs from the value that has been assumed for the design optimization. For instance, applying design 1B instead of 1A for a viscoelastic storage modulus of 0.1 GPa, leads to 42.5% less damping. On the other hand, applying design 1A instead of 1B for a storage modulus of 0.01 GPa, the modal loss factor is also 30.6% less. An exception can be observed for the third mode. Here, the inappropriate design (config. 3A) provides nearly the same damping for $E' = 0.01$ GPa as the appropriate design (config. 3B). The analysis shows that the final design of a CLD treatment is not only mode dependent, but also strongly dependent on the prevailing viscoelastic storage modulus.

5.2 Thermal influence on optimal design

In this section, the material properties presented in Figure 10 are applied for the viscoelastic material. An optimization is performed for the two previously mentioned temperatures. For this purpose, the IES has to be implemented in the process chain. Additionally, the number of design variables is set to eight. This means that for the first and second bending mode (distribution approach (3)), each design variable encompasses ten elements (e.g. DV1: 1-5 + 76-80). The distribution for the third bending mode follows approach (2) with a distribution schema presented in Table 6.

Table 6: Design variable distribution for the third bending mode

DV1	DV2	DV3	DV4
1-5 + 76-80	6-11 + 70-75	12-17 + 64-69	18-23 + 58-63
DV5	DV6	DV7	DV8
24-28 + 53-57	29-34 + 47-52	35-37 + 44-46	38-43

The results of the optimization runs are presented in Table 7. Config. C corresponds to a layout temperature of -20°C, while config. D corresponds to a temperature of 20°C. It can be seen that the designs for both configurations are almost oppositional. This applies in particular for the first and second mode. For instance, the optimal design of the first mode changed from a “rolling pin” shape to a “dumbbell” shape.

Table 7: Comparison of optimal designs for different temperatures

Mode	Config.	Optimal design	Modal loss factor [-] $T = -20°C$	Modal loss factor [-] $T = 20°C$
1.	C		0.2122	0.0720
	D		0.0972	0.1572
2.	C		0.2128	0.0641
	D		0.1051	0.1080
3.	C		0.1892	0.0563
	D		0.0970	0.0792

The values of the modal loss factor underline the observations from Section 5.1: The design, optimized for a specific temperature, offers significantly less damping performance when operating at a different temperature. By looking at Figure 12, it gets clear that this effect is not mainly caused by different material loss factors, prevailing at the corresponding eigenfrequencies. For -20°C (a), the material loss factor of the second and third bending mode of configuration C is lower than for configuration D. Nevertheless, the modal loss factor for these modes is significantly higher in case of configuration C. The same applies to the second bending mode at 20°C (b). Although the material loss factor is higher for configuration C, the damping performance of configuration D is superior.

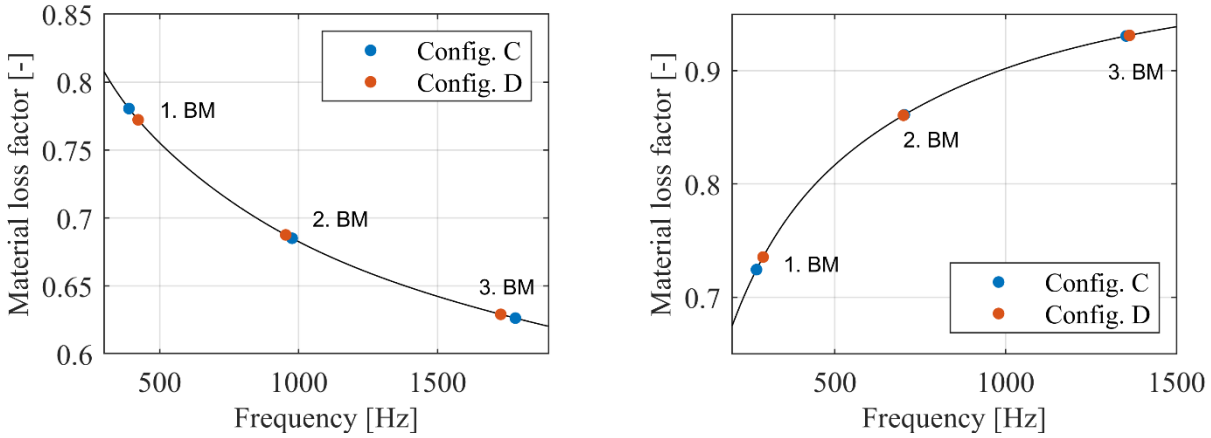

Figure 11: Material loss factors at eigenfrequencies of first three bending modes (BM) for (a) -20°C and (b) 20°C. It should be noted that the horizontal axis is plotted in linear scale.

From these observations it can be concluded that the storage modulus changes have a greater impact on the vibration damping than the material loss factor. In fact, a higher material loss factor does not compensate for an inappropriate design.

As a consequence, it is not sufficient to tune only the eigenfrequencies of a vibrating CLD system regarding the glass transition temperature of a viscoelastic material. Instead, more effort needs to be invested to establish an appropriate shear stiffness of the additional CLD layers. This objective is difficult to accomplish, if the operating boundary temperatures are far apart from each other. In this context, the nodes and antinodes of a mode shape play an important role for a rule of thumb of an appropriate design. In the considered case it is beneficial to design wide layers on locations of antinodes and slim layers on nodes or free ends for low temperature. Exactly the opposite applies for high temperatures.

However, it is emphasized that the optimal design is additionally sensitive to other system and structural parameters, such as layer thicknesses or boundary condition. Any modification has an influence on the resulting structural behavior and requires a detailed analysis of the corresponding optimal design.

5.3 Experimental validation

The transferability of the numerically determined design to real structures is experimentally validated. In this context, the optimal design configuration 1.D (see Table 7Table 7) has been chosen for validation and the corresponding parts of host structure, core and face layer have been manufactured accordingly. The metallic layers are made of aluminum and their thicknesses and material properties correspond to Table 1. The elastomeric layer was cut out of a vulcanized bromobutyl rubber mat. Since rolling of the elastomer compound prior to vulcanization is not a highly precise manufacturing technique, the thickness of the elastomeric strip is slightly inhomogeneous, differing between 1.85 mm at one end and 2 mm at the other end. After assembling the sandwich by conglutinating the layers with Loctite 480, the total thickness of the CLD beam differs between 15.08 mm and 15.18 mm. This means that the adhesive contributes with approximately 0.2 mm to the total thickness of the CLD laminate. While the influence of the adhesive is

neglected, the thickness of the viscoelastic layer is assumed to be constant and is set to 1.9 mm in the numerical simulation.

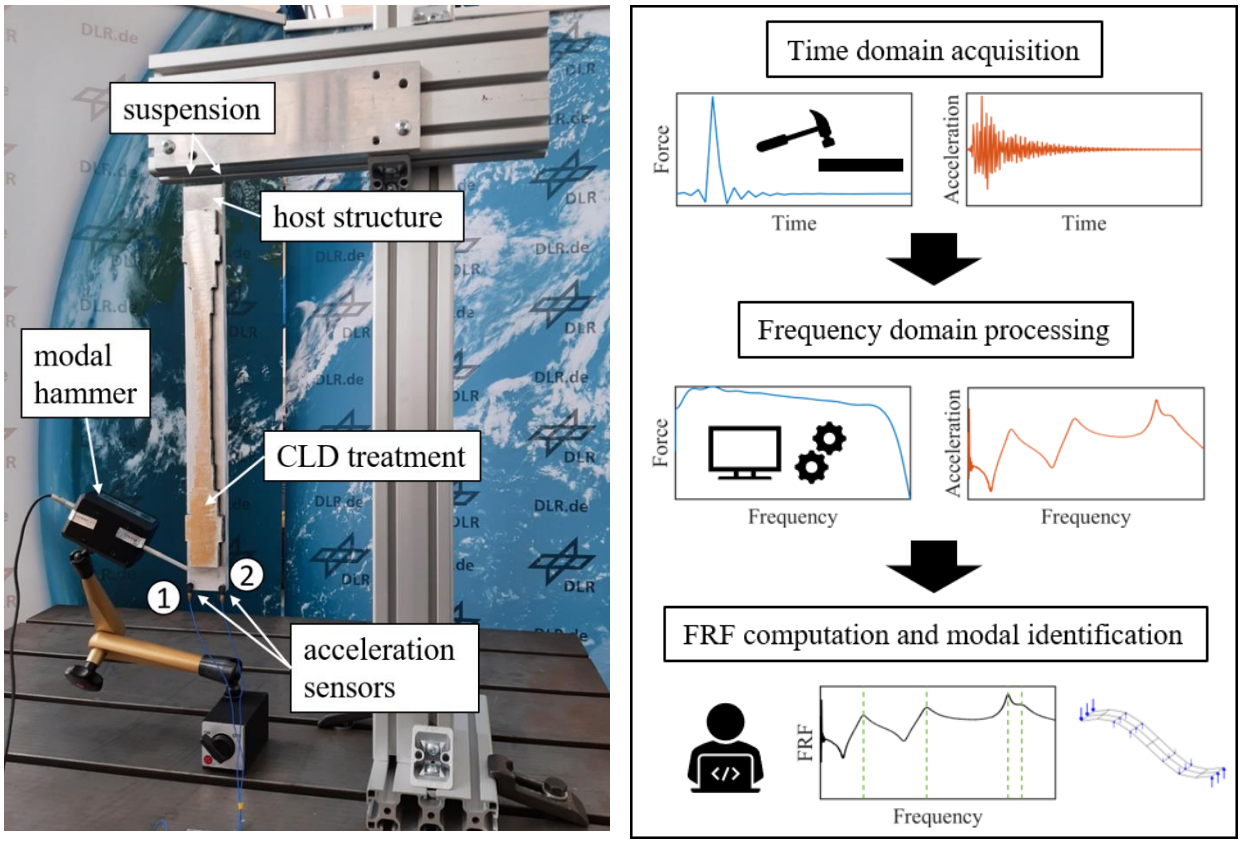

(a) (b)

Figure 12: (a) Experimental setup of the impact test and (b) process chain of experimental modal analysis

Figure 12 shows the experimental setup of the modal test. The measurement is performed at ambient temperature of 20°C. The sandwich beam is suspended at one end and two acceleration sensors are added on the other end. Similar tests have been conducted on previous samples using a scanning laser-vibrometer. Therefore, the mode shapes and their order of sequence are known in general. Since the test was not conducted in a climate chamber but instead in a laboratory with uncontrolled ambient temperature, it was desired to have a short duration of the experiment. Eigenfrequencies and damping ratios for bending and torsion modes have to be identified. Consequently, at least two response sensors are necessary in order to distinguish between bending and torsion modes. The structure is excited by an automated modal hammer and the force and acceleration time data is acquired. As a driving point, the back side of the position of sensor 1 is chosen. In a next step, the time data is processed by a rectangular window for the force channel and by an exponential window for the response channels. Afterwards, a Fast Fourier Transformation is applied and the corresponding power spectral densities are determined. The frequency response functions (FRFs) are calculated and averaged for multiple impacts (in total 10). Finally, the PolyMAX algorithm of the Siemens Testlab software is used to identify the eigenfrequencies, modal damping ratios and mode shapes from the FRFs. The PolyMAX algorithm is a multiple degrees of freedom frequency-domain identification method that is based on the least-squares principle and explained in [42]. The common procedure and the mathematical methods for signal processing and experimental modal analysis are well documented in [38].

Figure 13 illustrates a Bode plot of the host structure (undamped beam) compared to the CLD configuration. It is evident that the additional CLD layers significantly attenuate the resonance peaks. The damping effect can also be identified by means of wider resonance peaks and flatter slopes of the phase response when passing a resonance. Due to the changes of mass and stiffness, the order of the third bending (3. BM) and torsion (1. TM) mode changed compared to the undamped beam. Furthermore, some tiny peaks appear which correspond to the transverse bending modes. These modes are hardly visible, since the structure is

only weakly excited in transverse direction and the sensor measured little response due to the transverse sensitivity (i.e. cross talk) of the acceleration sensors used.

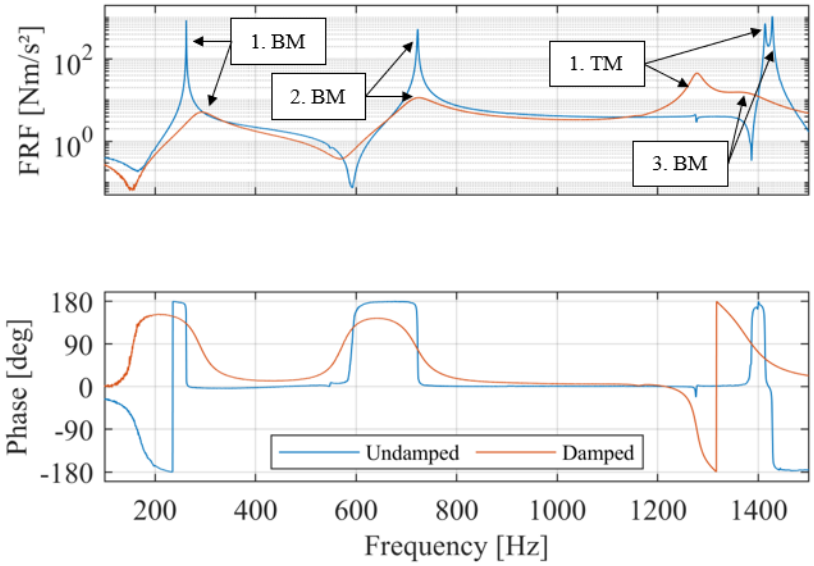

Figure 13: Bode plot of Sensor 2 for the undamped and damped beam

The comparison of eigenfrequencies and damping ratios between simulation and experimental data can be found in Table 8. It is striking that the eigenfrequencies correlate with considerable accuracy ($\Delta f < 1\%$). In opposite, the simulated damping ratios slightly deviate from the identified damping. The simulated damping is always underestimated for the bending modes. The deviation of damping has different reasons. On the one hand, the damping ratio is known as a very sensitive parameter in modal identification and strongly depends on the evaluation bandwidth and on the level of excitation of a mode shape (i.e. modal participation). On the other hand, the PolyMAX algorithm fits the synthetic FRF based on the linear viscous damping model. As a consequence, the frequency dependence of the viscoelastic material damping is not considered, leading to an erroneous identification which reflects the best possible viscous damping fit to a structure having frequency dependent hysteretic damping. However, the state of the art does not provide an identification method dedicated for viscoelastic damping. In addition, similar damping and even larger deviations are reported e.g. by Kim et al. [17] and Leibowitz and Lifshitz [43]. Under these circumstances, a damping deviation of 6.93 % and less is assumed as acceptable and the numerical prediction is considered as validated.

Table 8: Comparison of simulation and experimental data of bending modes

Mode	Modal parameter	Simulation	Experiment	Deviation [%]
1. bending mode	Eigenfrequency [Hz]	291.4	289.2	0.76
	Damping [%]	7.92	8.51	-6.93
2. bending mode	Eigenfrequency [Hz]	719.9	719.1	0.11
	Damping [%]	3.90	4.11	-5.11
3. bending mode	Eigenfrequency [Hz]	1377	1376	0.07
	Damping [%]	2.99	3.13	-4.47

The experimental validation has proven that the damping performance can be significantly improved by the proposed optimization method. Keeping in mind that the simulation is based on a rather complex, frequency- and temperature-dependent viscoelastic material model, it is also remarkable that the modal parameters resulting from both numerical and experiment are in good accordance.

6 Conclusion

A novel, gradient-free approach for shape optimization was presented and applied to the viscoelastic damping optimization of CLD beams at different temperatures. Based on a Gauss-Seidel method, the algorithm was able to sequentially determine the width of the viscoelastic core and the face layer, taking into account a mass constraint. The FE mesh of the host structure remained unchanged during the analysis. The numerical effort of the method can be reduced by merging individual element sections as design variables and by using symmetry effects of considered mode shapes.

In a numerical analysis it was shown that the optimal design depends on the viscoelastic storage modulus since the shear stiffness of the viscoelastic layer is determined by the storage modulus. Furthermore, as the storage modulus is strongly temperature-dependent, the optimal design also turns out to be dependent on temperature. This was demonstrated and experimentally validated using a fully characterized, frequency- and temperature-dependent elastomer compound. The results show that the optimal designs for two different ambient temperatures can be completely different from each other. For a low temperature, it is more beneficial to place wide CLD layers at locations of antinodes, while for high temperatures wide CLD layers should be added on vibration nodes of the host structure. In practice, the damping performance of the optimal design has its maximum at the design temperature, and the damping performance is smaller for off-design temperatures. As a consequence, design optimizations must take these considerations into account. If for example, we attempt to increase the storage modulus by modifications of the material properties in such a way that its glass temperature is close to the operation temperatures, it might happen that the shear stiffness of the viscoelastic layer is affected and the overall performance decreases.

The present findings are particularly important for viscoelastic damping design of aircraft structures. Different vibration problems occur at different airframe components. For example, passive damping of the wings has the potential to increase aeroelastic stability and pushes the flutter critical speed further upwards. In addition, increased damping of wings is beneficial for passive load alleviation like in case of gust encounter. Also, the increase of damping is beneficial for the fatigue life of the wings. For aircraft fuselage, passive damping by viscoelastic materials contributes to the acoustic comfort inside the cabin. Structure borne-noise emerging from different sources can efficiently be dissipated. However, it has to be considered that during operation of an aircraft, the airframe will pass through different temperature levels. Possible improvements of the presented method encompass the inclusion of further design parameters such as the layer thicknesses of the core and face layer and the adaption to plate structures. In order to mitigate the problem of reduced damping performance at different temperatures, the shape optimization algorithm can incorporate these temperatures into the objective function.

Acknowledgements

We would like to acknowledge the funding by the Deutsche Forschungsgemeinschaft (DFG, German Research Foundation) under Germany's Excellence Strategy – EXC 2163/1- Sustainable and Energy Efficient Aviation – Project-ID 390881007.

Furthermore, we would like to acknowledge the support of our colleague Tobias Meier who was taking over the manufacturing of the core and face layer and the assembly with the host structure.

Appendix

Table A: Model parameters of the generalized Maxwell Model of the elastomer compound

	Index i						
Parameter	1	2	3	4	5	6	7
$\tau_i\ [s]$	1.000e+04	3.162e+03	1.000e+03	3.162e+02	1.000e+02	3.162e+01	1.000e+01
$G_i\ [Pa]$	4.045e+04	4.276e+04	5.985e+04	7.428e+04	5.995e+04	7.379e+04	7.967e+04
	8	9	10	11	12	13	14
$\tau_i\ [s]$	3.162e+00	1.000e+00	3.162e-01	1.000e-01	3.162e-02	1.000e-02	3.162e-03
$G_i\ [Pa]$	8.387e+04	1.049e+05	1.250e+05	1.614e+05	2.278e+05	3.341e+05	5.495e+05
	15	16	17	18	19	20	21
$\tau_i\ [s]$	1.000e-03	3.162e-04	1.000e-04	3.162e-05	1.000e-05	3.162e-06	1.000e-06
$G_i\ [Pa]$	1.002e+06	1.962e+06	3.824e+06	7.580e+06	1.526e+07	2.651e+07	4.224e+07
	22	23	24	25	26	27	inf
$\tau_i\ [s]$	3.162e-07	1.000e-07	3.162e-08	1.000e-08	3.162e-09	1.000e-09	-
$G_i\ [Pa]$	5.911e+07	6.895e+07	9.909e+07	1.610e+08	1.164e+02	2.538e-01	7.473e+05

Table B: WLF and Arrhenius parameters of the elastomer compound for horizontal and vertical shifting

C1 [-]	C2 [K]	T_{ref} [K]	$b_{T,E'}$ [J/mol]	$b_{T,E'}$ [J/mol]
7.26	166.25	293.15	2010	2010

References

[1] M. D. Rao, „Recent applications of viscoelastic damping for noise control in automobiles and commercial airplanes," *Journal of Sound and Vibration,* Bd. 262, p. 457–474, 2003.

[2] H. Oberst und K. Frankenfeld, „Über die Dämpfung der Biegeschwingungen dünner Bleche durch fest haftende Beläge," *Acustica,* Bd. 2, p. 181–194, 1952.

[3] E. M. Kerwin, „Damping of Flexural Waves by a Constrained Viscoelastic Layer," *The Journal of the Acoustical Society of America,* Bd. 31, p. 952–962, 1959.

[4] D. Ross, E. E. Ungar und E. M. Kerwin, „Damping of plate flexural vibrations by means of viscoelastic laminate," *Structural Damping,* p. 49–88, 1959.

[5] R. A. Di Taranto, „Theory of vibratory bending for elastic and viscoelastic layered finite-length beams," *ASME Journal of Applied Mechanics,* Bd. 32, p. 881–886, 1965.

[6] D. J. Mead und S. Markus, „The forced vibration of a three-layer, damped sandwich beam with arbitrary boundary conditions," *Journal of Sound and Vibration,* Bd. 10, p. 163–175, 1969.

[7] D. K. Rao, „Frequency and loss factors of sandwich beams under various boundary conditions," *Journal of Mechanical Engineering Science,* Bd. 20, p. 271–282, 1978.

[8] J. M. Lifshitz und M. Leibowitz, „Optimal sandwich beam design for maximum viscoelastic damping," *International Journal of Solids and Structures,* Bd. 23, p. 1027–1034, 1987.

[9] J.-L. Marcelin, P. Trompette und A. Smati, „Optimal constrained layer damping with partial coverage," *Finite Elements in Analysis and Design,* Bd. 12, pp. 273-280, 1992.

[10] J.-L. Marcelin, S. Shakhesi und F. Pourroy, „Optimal constrained layer damping of beams: Experimental and numerical studies," *Shock and Vibration,* Bd. 2, p. 445–450, 1995.

[11] K. Svanberg, „The method of moving asymptotes - A new method for structural optimization," *International Journal for Numerical Methods in Engineering,* Bd. 24, pp. 359-373, 1987.

[12] M. Alvelid, „Optimal position and shape of applied damping material," *Journal of Sound and Vibration,* Bd. 310, p. 947–965, 2008.

[13] G. Lepoittevin und G. Kress, „Optimization of segmented constrained layer damping with mathematical programming using strain energy analysis and modal data," *Materials & Design,* Bd. 31, pp. 14-24, 2010.

[14] A. L. Araújo, P. Martins, C. M. M. Soares, C. A. M. Soares und J. Herskovits, „Damping optimization of viscoelastic laminated sandwich composite structures," *Structural and Multidisciplinary Optimization,* Bd. 39, p. 569–579, 2009.

[15] J. F. A. Madeira, A. L. Araújo, C. M. M. Soares, C. A. M. Soares und A. J. M. Ferreira, „Multiobjective design of viscoelastic laminated composite sandwich panels," *Composites Part B: Engineering,* Bd. 77, p. 391–401, 2015.

[16] Z. Ling, X. Ronglu, W. Yi und A. El-Sabbagh, „Topology optimization of constrained layer damping on plates using Method of Moving Asymptote (MMA) approach," *Shock and Vibration,* Bd. 18, p. 221–244, 2011.

[17] S. Y. Kim, C. K. Mechefske und I. Y. Kim, „Optimal damping layout in a shell structure using topology optimization," *Journal of Sound and Vibration,* Bd. 332, p. 2873–2883, 2013.

[18] W. Zheng, Y. Lei, S. Li und Q. Huang, „Topology optimization of passive constrained layer damping with partial coverage on plate," *Shock and Vibration,* Bd. 20, p. 199–211, 2013.

[19] Z. Fang und L. Zheng, „Topology Optimization for Minimizing the Resonant Response of Plates with Constrained Layer Damping Treatment," *Shock and Vibration,* Bd. 2015, 2015.

[20] D. Zhang, T. Qi und L. Zheng, „A hierarchical optimization strategy for position and thickness optimization of constrained layer damping/plate to minimize sound radiation power," *Advances in Mechanical Engineering,* Bd. 10, p. 1–15, 2018.

[21] M. Gröhlich, M. Böswald und R. Winter, „Finite element optimization of viscoelastic damping applications," in *Proceedings of ISMA 2020 International Conferenceon Noise and Vibration Engineering, Leuven, Belgium,* 2020.

[22] A. D. Nashif, D. I. Jones und J. P. Henderson, Vibration damping, New York: John Wiley & Sons, 1985.

[23] H. F. Brinson und L. C. Brinson, Polymer Engineering Science and Viscoelasticity, Springer, 2008.

[24] D. A. Rade, J.-F. Deü, D. A. Castello, A. M. G. de Lima und L. Rouleau, „Passive vibration control using viscoelastic materials," in *Nonlinear Structural Dynamics and Damping. Mechanisms and Machine Science*, Bd. 69, Springer, Cham, 2019, p. 119–168.

[25] B. C. Chakraborty und D. Ratna, Polymers for Vibration Damping Applications, Elsevier, 2020.

[26] C. M. A. Vasques, R. A. S. Moreira und J. D. Rodrigues, „Viscoelastic Damping Technologies - Part I: Modeling and Finite Element Implementation," *Journal of Advanced Research in Mechanical Engineering*, Bd. 1, p. 76–95, 2010.

[27] X. Q. Zhou, D. Y. Yu, X. Y. Shao, S. Q. Zhang und S. Wang, „Research and applications of viscoelastic vibration damping materials: A review," *Composite Structures*, Bd. 136, pp. 460-480, 2016.

[28] R. L. Bagley und P. J. Torvik, „Fractional calculus - A different approach to the analysis of viscoelastically damped structures," *AIAA Journal*, Bd. 21, p. 741–748, 1983.

[29] D. F. Golla und P. C. Hughes, „Dynamics of Viscoelastic Structures - A Time-Domain, Finite Element Formulation," *Journal of Applied Mechanics*, Bd. 52, p. 897–906, 1985.

[30] M. L. Williams, R. F. Landel und J. D. Ferry, „The temperature dependence of relaxation mechanisms in amorphous polymers and other glass-forming liquids," *Journal of the American Chemical Society*, Bd. 77, p. 3701–3707, 1955.

[31] A. R. Payne, „The dynamic properties of carbon black-loaded natural rubber vulcanizates. Part I," *Journal of Applied Polymer Science*, Bd. 6, p. 57–63, 1962.

[32] A. R. Payne, „The dynamic properties of carbon black loaded natural rubber vulcanizates. Part II," *Journal of Applied Polymer Science*, Bd. 6, p. 368–372, 1962.

[33] J. Fritzsche und M. Klüppel, „Structural dynamics and interfacial properties of filler-reinforced elastomers," *Journal of Physics: Condensed Matter*, Bd. 23, p. 035104, 2011.

[34] M. Gröhlich, A. Lang, M. Böswald und J. Meier, „Viscoelastic damping design - Thermal impact on a constrained layer damping treatment," *Materials & Design*, p. 109885, 2021.

[35] K. J. Bathe, Finite Element Procedures, Prentice Hall, 1996.

[36] L. Rouleau, J.-F. Deü und A. Legay, „A comparison of model reduction techniques based on modal projection for structures with frequency-dependent damping," *Mechanical Systems and Signal Processing*, Bd. 90, p. 110–125, 2017.

[37] M. Gröhlich, M. Böswald und R. Winter, „An Iterative Eigenvalue Solver for Systems with Frequency Dependent Material Properties," in *Proceedings of the DAGA 2020, Hannover, Germany*, 2020.

[38] D. J. Ewins, Modal Testing: theory, practice and application, Research Studies Press Ltd., 2000.

[39] N. Kumar und S. P. Singh, „Vibration control of curved panel using smart damping," *Mechanical Systems and Signal Processing*, Bd. 30, p. 232–247, 2012.

[40] M. Gröhlich, M. Böswald und R. Winter, „Frequency and temperature dependent viscoelastic vibration damping capability of a novel local CLD treatment," in *Proceeding of INTER-NOISE 2019*, Madrid, Spain, 2019.

[41] M. Gröhlich, M. Böswald und R. Winter, „Vibration damping capabilities of treatments with frequency and temperature dependent viscoelastic material properties," in *Proceedings of ICA 2019 - 23rd International Congress on Acoustics*, Aachen, Germany, 2019.

[42] B. Peeters, H. V. der Auweraer, P. Guillaume und J. Leuridan, „The PolyMAX frequency-domain method: anew standard for modal parameter estimation?," *Shock and Vibration*, Bd. 11, p. 395–409, 2004.

[43] M. Leibowitz und J. M. Lifshitz, „Experimental verification of modal parameters for 3-layered sandwich beams," *International Journal of Solids and Structures*, Bd. 26, p. 175–184, 1990.